A test experiment to measure sub-GeV flux in the on-axis direction at the J-PARC neutrino beam

December 18, 2009

Abstract

We propose to J-PARC PAC a test experiment of a detector to measure the low energy (E_ν<1 GeV) neutrino flux in the on-axis beam direction. This can be achieved by a tracking detector composed of interleaved layers of iron and scintillator bars. We expect that this test experiment can measure low energy part of the J-PARC neutrino flux. We performed Monte Carlo simulation studies using the on-axis beam flux and demonstrated that the detector can measure the low energy component of the beam with good performance.

Proponents

LHEP, University of Bern, Switzerland:
A. Ariga, T. Ariga, F. Bay, A. Ereditato, E. Frank, R. Haenni, F. Juget, I. Kreslo, P. Lutz, R. Mathieu, M. Messina, U. Moser, C. Pistillo, B. Rossi.

IN2P3, IPN Lyon, France:
D. Autiero, B. Carlus, A. Cazes, L. Chaussard, Y. Declais, S. Gardien, C. Girerd, C. Guerin, J. Marteau, E.Pennacchio

ICRR, University of Tokyo, Japan:
C. Ishihara, H. Kaji, T. Kajita[†], K. Kaneyuki, K. Okumura[‡], Y. Shimizu, N. Tanimoto

[†] : project leader

[‡] : on-site contact person

Contents

1 Introduction

We propose a test experiment to measure low energy neutrino events with a simple detector system. We expect that this experiment can provide information on sub-GeV neutrino flux at the J-PARC neutrino beam line. The information can be useful for the neutrino experiment, such as T2K, to be carried out in this beam line.

We intend to install a new detector on the SS (Service Stage) floor of the ND280 hall, where the INGRID horizontal arrays are located. A candidate place is in front of the INGRID horizontal modules, which will be right next to one of the INGRID off-diagonal detector, as shown in Figure 1. The installation place is

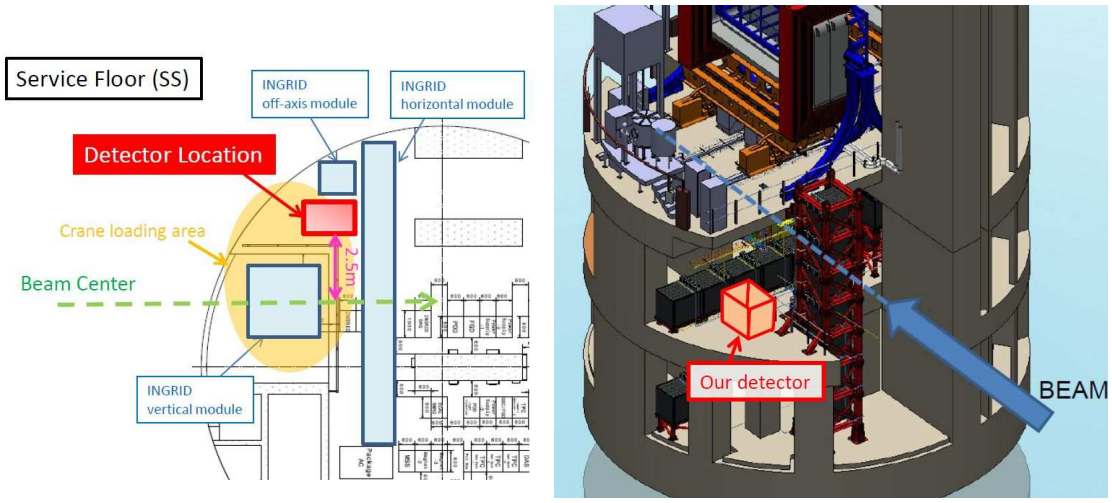

Figure 1: The floor plan for the SS floor (left) and the 3D view of the ND280 hall (right) are shown. In both figures, the red box shows the candidate place to install the detector. The detector will be placed in front of the INGRID horizontal modules.

in the loading area of the crane. This place is 2.5 meter apart from the center of the beam where off-axis angle is 0.5. In Figure 2, the energy spectrum of neutrino interaction modes at the detector location is shown. Our detector has a total mass of about 5.7 ton. Therefore, it can be installed with the 10 ton crane of the ND280 hall and be uninstalled quickly upon request.

In this proposal, we show the detector design including readout electronics, the expected performance from Monte Carlo simulations, and the construction and installation schedule.

2 Detector design

The proposed detector is made of iron and counter planes, both 1 cm thick, as shown in Figure 3. The detector size is 108 cm width $\times$ 108 cm height $\times$ 185 cm length, for a total mass of about 5.7 ton. It consists of 50 square iron plates, each followed by a counter plane. The detector is surrounded by veto scintillator planes. The counter plane consists of 20 plastic scintillator bars. The size of a scintillator bar is $5 \times 1 \times 100\,\mathrm{cm}^3$ and a 1 mm diameter wave length shifting (WLS) fiber is inserted into a hole in the bar. The WLS fiber is connected to an optical clear fiber to feed light to a Hamamatsu 64 channel multianode photomultiplier (PMT) at one end shown in Figure 4.

Each counter plane has a multi-layer structure. It consists of a 1 mm thick aluminum sheet $1060 \times 1015\ \mathrm{mm}^2$ in surface area, double sided scotch strips, a series of 20 scintillator bars, again double sided scotch strips on the scintillator bars and finally one more aluminum sheet to close up the counter plane structure. The double sided scotch strips and the aluminum sheet provide the counter plane with the desired mechanical rigidity. Figure 5 shows the multi-layer structure of the counter plane.

After the counter plane is assembled the fibers from the 20 scintillator bars are inserted into a black pipe that is glued to the cover and to the cookie. The intermediate fiber collector shown in Figure 6 is

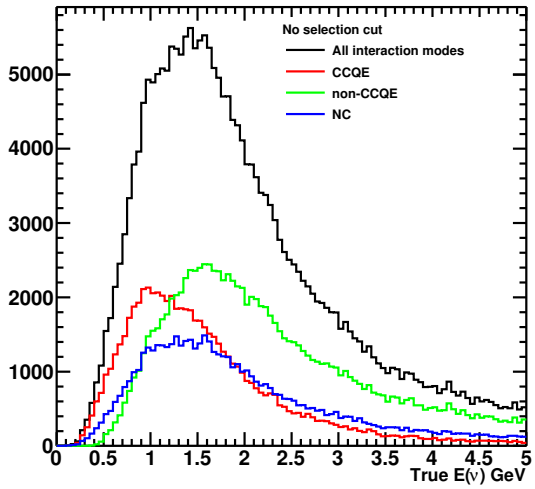

Figure 2: Neutrino energy distributions for interaction modes at the detector location 2.5 m apart from the beam center.

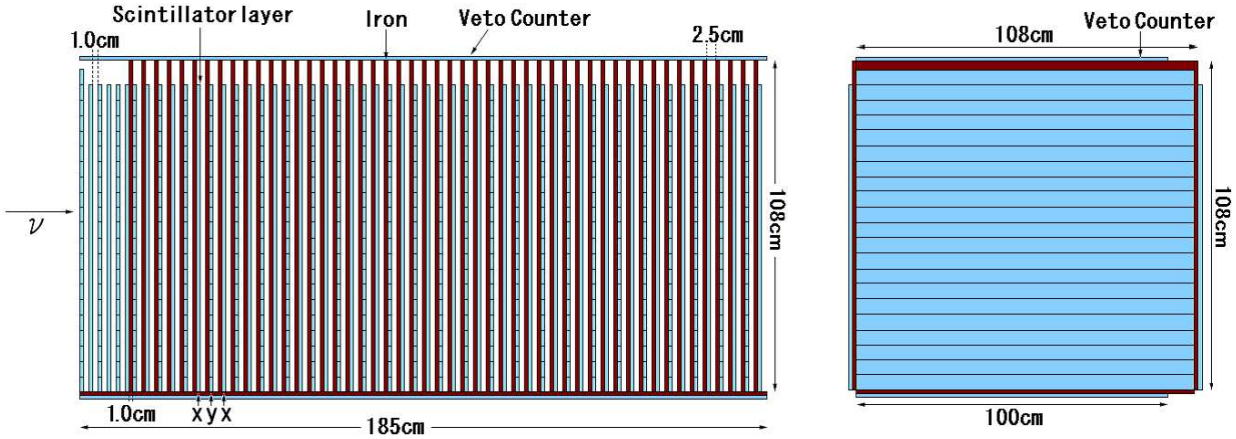

Figure 3: Schematic drawing (top and side view) of the proposed detector. The scintillator bars ($5 \times 100 \times 1$ cm^3) are displayed in blue and the iron plates in brown. The counter plane consists of 20 scintillator bars. The most upstream counter plane works as front veto and is larger than other counter planes. It consists of 21 long scintillator bars ($5 \times 108 \times 1$ cm^3). The size of the top, bottom, and side veto planes is $100 \times 185 \times 1$ cm^3 and they consist of 37 scintillator bars.

Figure 4: The 64 channel multianode PMT (H8804MOD-1) with alignment pins and a cookie.

installed on the same board where the electronic readout chain and PMT is mounted. It fits three cookies holding 20 fibers each into the single cookie holding the 60 fibers that are precisely matched to the PMT photocathode channels. The optical connection between the three bundles of 20 fibers and the single bundle of 60 fibers is made by clear fibers placed in the intermediate collector.

The iron plates and scintillator planes can be installed in a folder from the top of the module, the readout boards and PMTs are installed in readout boxes, and placed on the top of the detector. The detector is surrounded by veto scintillator planes in order to reject cosmic ray backgrounds and high energy neutrinos with energy > 1 GeV. A fully assembled module with veto planes and readout boxes is shown in Figure 7.

The DAQ system has been developed and running in the OPERA experiment. The Hamamatsu multianode PMT is known to have a low dark rate (10 Hz per pixel), so there will be no need to cool the system. Since only a few cables are connected to the readout system, it will be possible to swap the modules and perform comparison runs. This can be used to cancel out possible inter-calibration errors.

The readout chain is based on the concept of Ethernet capable smart sensors where data are acquired asynchronously, time-stamped and transmitted through a standard network to an event builder PC. This PC is offline and takes care of data sorting and time matching of hits belonging to the same time window with 10 ns accuracy. Each sensor (M64) is connected to two different electronics boards:

- an analog front-end board directly plugged to the PMT housing two 32-channel ASICs
- a digital motherboard including fast ADC, a high voltage module, a LED pulse generator, a clock decoding unit and a micro-processor daughterboard called "mezzanine" connected to the rest of the system via a standard Ethernet link.

The full PMT readout chain is displayed in Figure 8.

The main features of the analog and digital readout electronics, DAQ and event building system are:

- triggerless operation mode (to allow continuous recording of events)
- accurate timestamping locked on the GPS (to correlate off line events)
- continuous running capability
- low deadtime
- modular and flexible hardware/software architecture (trigger schemes, on line and off line filters etc).

The Ethernet capability makes the readout chain very compact and minimizes the cabling. The detector can be connected to the PC which will act as event builder with one Ethernet cable, one clock cable and

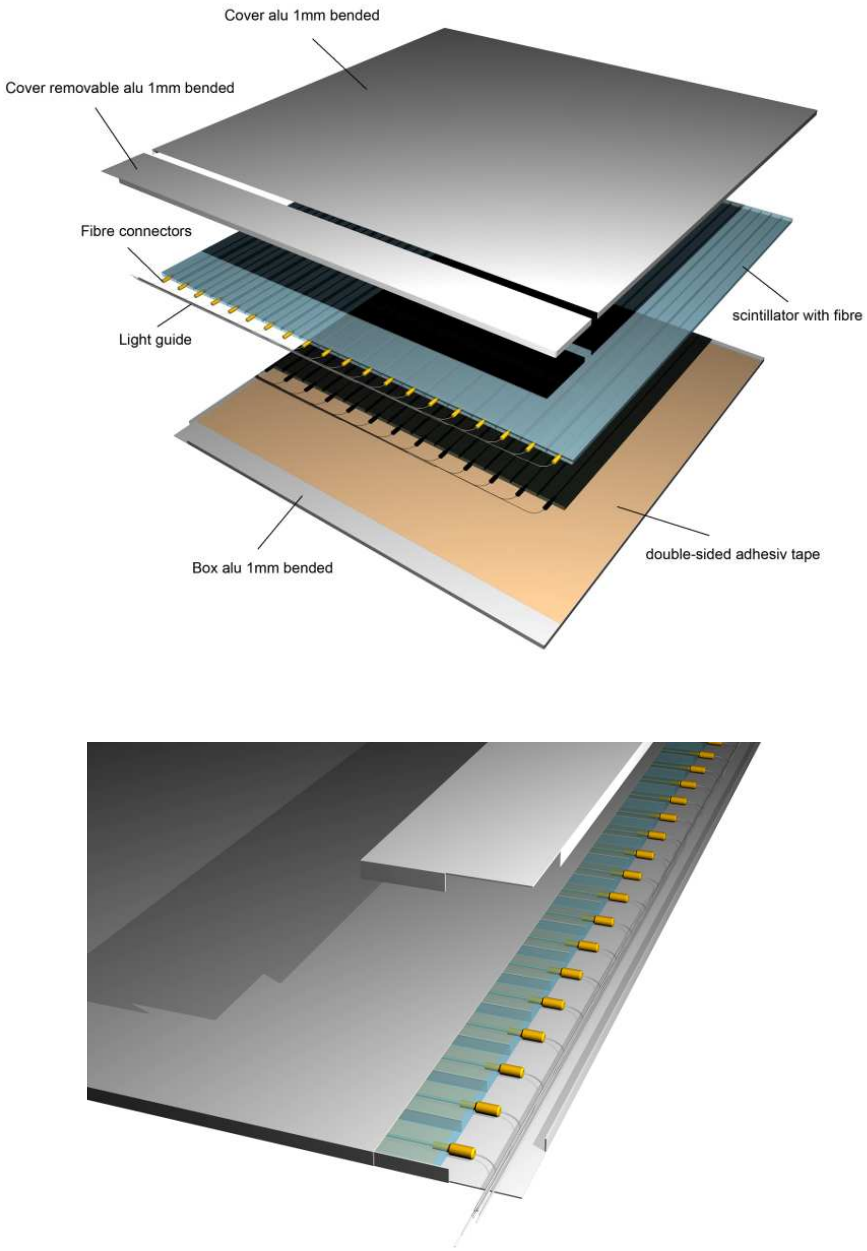

Figure 5: Details of the counter plane structure. Top drawing shows the inside of the counter plane with optical connectors and fibers. The bottom drawing shows the sandwich structure of the plane.

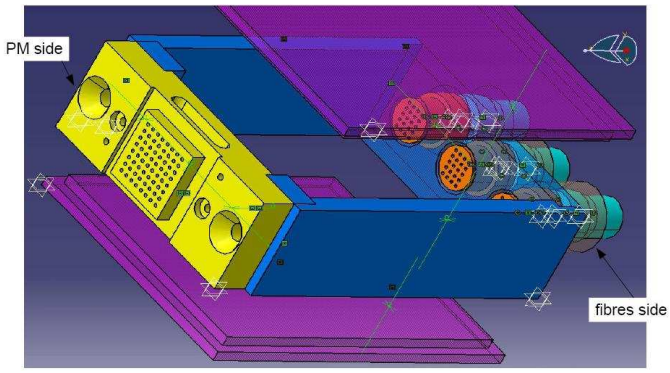

Figure 6: Intermediate light collector.

the low voltage cables. High voltages are generated locally on the cards. A network switch located on the module itself will interconnect the various cards. The module can be thus unplugged and moved very quickly and easily. All the software and graphical user interfaces for the control of the DAQ system, including remote WAN control and ROOT output, already exist and are well tested.

Figure 7: The detector fully assembled with veto planes and readout boxes.

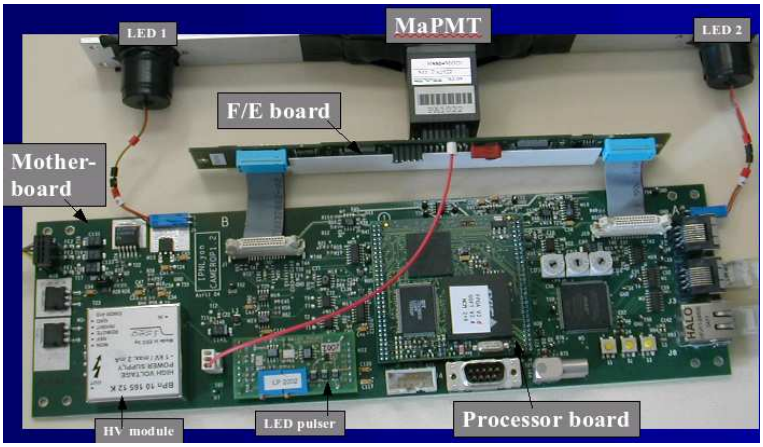

Figure 8: Picture of the complete PMT readout chain.

3 Detector performance

The peak energy of the neutrino flux is about 2 GeV. Above 1 GeV, the distribution is dominated by charged-current non-quasi elastic (CC non-QE) interaction. The proton track from neutral current (NC) interaction is mis-identified as a muon track. In order to reconstruct low energy neutrino events with $E_\nu < 1$ GeV, these should be rejected as much as possible.

We have generated Monte Carlo data using the on-axis beam flux but with the detector positioned slightly off-axis at 0.5 degrees. GEANT4 is used, and the neutrino interactions are generated based on the beam flux provided by the T2K beam group (version 07a) and the NEUT neutrino interaction code. The following cuts are applied,

1. Number of hit layers ($N_{HitLayer}$) ≥ 5.
2. No hits in the veto counter planes.
3. All hits are within the fiducial volume (FV).
4. $N_{p.e.}^{tail} \times \cos\theta_{\mu} < 85$.
5. $N_{2HitLayer} \leq 2$.
6. $p_{\mu} > 250$ MeV/c.

The cuts 3, 4, 5, and 6 are implemented to retain low energy events and suppress contamination of high energy events because of the following reasons :

- For events generated via CC non-QE interactions, which are dominant in the energy region above 1 GeV, the reconstructed neutrino energy tends to be lower than the true energy because pions generated by neutrinos are difficult to be identified. The contamination from CC non-QE events in the energy region below 1 GeV is expected to increase.
- The interactions of high energy neutrinos tends to produce scattered nucleus with large momentum, which makes large numbers of hit layers. These tracks mis-identified as muon tracks, and the rate of NC events is increased in the on-axis measurements.
- Events with large momentum muons (>1 GeV) usually don't stop and go through the detector. Most of the events can be rejected by requiring there be no hits in the veto planes. However, these "partially contained" (PC) events can sneak into to the "fully contained" (FC) sample, since only 95 % of the solid angle is covered by the veto planes. This rate cannot be negligible in the on-axis measurement.

Figure 9 shows $N_{HitLayer}$ distributions for proposed installation place. The hits of CC interaction are due to scattered muon while those of NC are due to scattered proton. Therefore, $N_{HitLayer}$ for NC interaction is relatively smaller than that of CC. We applied $N_{HitLayer} \geq 5$ selection to reject NC events.

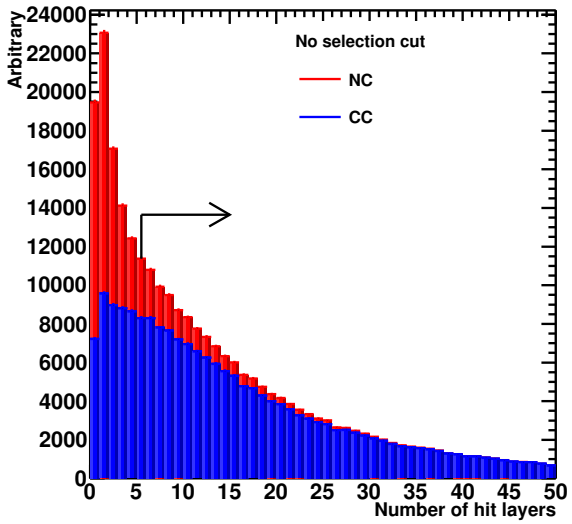

Figure 9: The number of hit counter layers, $N_{HitLayer}$, for both CC (blue) and NC interactions. The $N_{HitLayer}$ for NC is relatively smaller than that of CC. To reduce contamination of the NC events, we apply $N_{HitLayer} \geq 5$ selection.

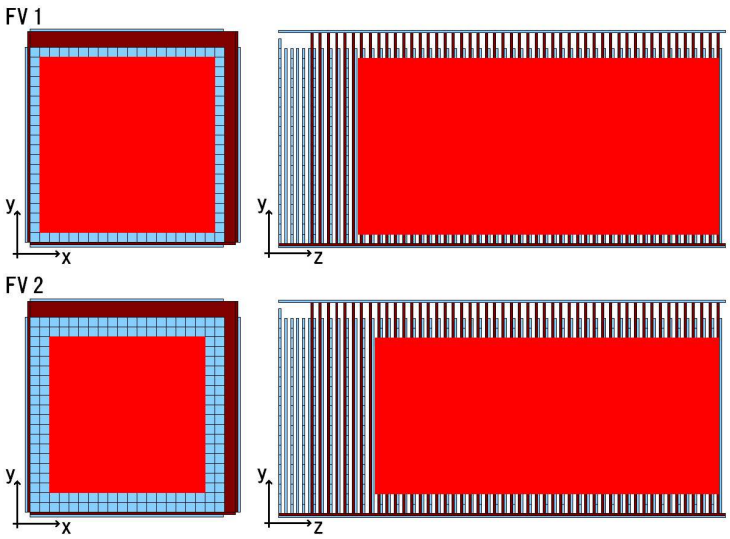

Figure 10: Fiducial volume (FV) definition. FV2 is for the events which the number of hit layer is in 5-9, and FV1 is greater than 9.

We applied that all hits must be within the fiducial volume (Figure 10) in cut 3. This selection is to perform tight reduction of PC events, which are mis-identified as the FC events due to the insufficient coverage of the veto counters.

Figure 11 shows the $N_{p.e.}^{tail} \times \cos\theta_\mu$ distribution, where $N_{p.e.}^{tail}$ is the number of photo-electrons measured in the last four layers of the track and θ_μ is the muon scattering angle with respects to the neutrino direction. This cut is added in order to reject events with single proton track generated via NC interactions. At the tail of the track, the ionization loss of proton is larger than that of muons. Therefore, NC events with single track proton have high $N_{p.e.}^{tail}$. Also protons tend to be scattered in the forward direction unlike muons. We apply a cut of $N_{p.e.}^{tail} \times \cos\theta_\mu < 85$. Figure 12 shows a typical single proton track event. Photo-electrons deposited in the last four layers were 38, 31, 33 and 37, and $N_{p.e.}^{tail} \times \cos\theta_\mu$ was 113.5.

The CC non-QE events have relatively high neutrino energy and produce multi-track events caused by muons and other secondary particles, such as pions. Figure 13 shows the event display of a typical multi-track CC non-QE event. Two tracks generated by a muon and a pion are seen. Proton in CCQE can produce a track sometimes, but the track length is relatively short. In order to reduce the fraction of CC non-QE events, the number of layers having 2 or more hits ($N_{2HitLayer}$) is applied. Figure 14 shows $N_{2HitLayer}$ distribution for each interaction mode. $N_{2HitLayer}$ for CC non-QE events becomes larger than that for CC QE due to multiple track generation. Events with $N_{2HitLayer} \leq 2$ are selected as single track candidates.

For a further rejection of NC events, we apply a cut at $p_\mu > 250$ MeV/c, where p_μ is the reconstructed muon momentum shown in Figure 15. Reconstructed tracks for NC events are mainly originated from protons, not muons, so the momentum tends to be low.

Figure 16 shows a typical CCQE event surviving all the selection cuts. A muon makes a clear single track and stops in the detector. The muon momentum is 655 MeV/c and reconstructed to be 644 MeV/c.

The muon range is determined by counting both the number of consecutive hit layers and measuring the direction of the muon track. The θ_x and θ_y angles with respect to the beam direction are used to calculate the angle between the track and the beam

$$\tan^2\theta_\mu = \tan^2\theta_x + \tan^2\theta_y. \tag{1}$$

The muon range is then proportional to $N_{\mathrm{HitLayer}}/\cos\theta_\mu$. The reconstructed muon momentum is determined by the following function

$$P_\mu^{\mathrm{rec}} = 15.3 \times \frac{N_{\mathrm{HitLayer}}}{\cos\theta_\mu} + 87.2\ [\mathrm{MeV}/c^2], \tag{2}$$

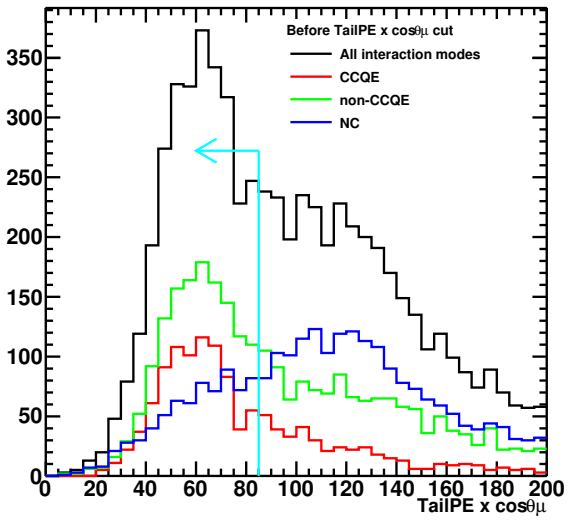

Figure 11: The $N_{p.e.}^{tail} \times \cos\theta_\mu$ distribution for CCQE (red), CC non-QE (green) and NC (blue) events. The NC events have large $N_{p.e.}^{tail}$ since the ionization loss of protons is larger than that of muons. We applied a cut of $N_{p.e.}^{tail} \times \cos\theta_\mu < 85$.

where the coefficients correspond to the energy loss in each layer (1 cm of iron and 1 cm of scintillator), which are obtained by the MC study. Figure 17 shows the true muon momentum for the events with no cuts applied, true and reconstructed one surviving all cuts. A certain amount of CC non-QE events still remain in the final sample. These events are either pions are absorbed in the nuclei, or pion momentum is too low to be identified as a secondary track in the detector. Before any selections applied, a large amount of events fall in the > 1 GeV region for the true momentum distribution; however, they can be reconstructed as < 1 GeV events since they are PC events. These PC events can be rejected by no veto hit and track in FV requirements effectively. Figure 18 shows the distributions of the reconstructed muon momentum as a function of the true muon momentum for all modes and the CCQE mode only. The resolution is defined as $(true - reconstructed)/true$ muon momentum. It indicates that the muon momentum can be well reconstructed using the detector with 6% resolution.

Figure 19 shows the true and reconstructed neutrino energy distributions for the final sample. The neutrino energy is reconstructed by using the reconstructed muon momentum and the scattering angle of the muon with respect to the beam direction as follows

$$E_\nu = \frac{1}{2} \cdot \frac{2M_p E_\mu - M_\mu^2}{M_p - E_\mu + \sqrt{E_\mu^2 - M_\mu^2} \cdot \cos\theta_\mu}, \tag{3}$$

where M_p and M_μ are the masses of proton and muon, respectively. E_μ and θ_μ are the energy and the scattering angle of the final state muon. Though there are some remaining events with $E_\nu^{true} > 1$ GeV that originate from CC non-QE and NC interactions, the reconstructed energy falls below 1 GeV. The mean reconstructed energy of the final sample is 0.49 GeV excluding the NC events. The r.m.s. spread of the true energy for the CC events is 0.347 (the events below 2 GeV are considered). As shown in Figure 20, the efficiency for CC-QE, CC non-QE, and NC events is plotted, the proposed detector has a reasonable acceptance for CC QE events below 1 GeV compared to other interaction modes, and features the significant reduction of performance for CC non-QE and NC events above 1 GeV energy region.

The number of remaining events after each selection step is summarized in Table 1. The total efficiency is 0.81 %, while those of CC QE, CC non-QE and NC events are 1.1 %, 0.62 % and 0.91 %, respectively. Note that these small efficiencies are due to the selection of low energy events over a large number of high

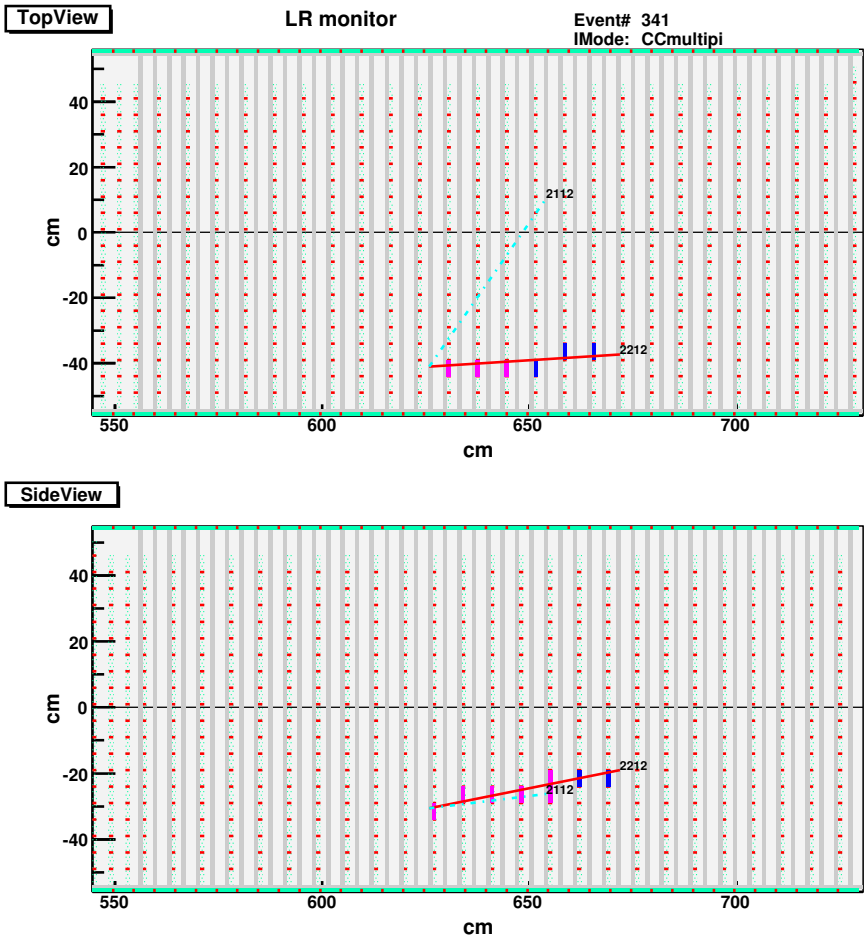

Figure 12: An event display of a single proton track event generated via charged current multiple pion interaction. The upper display shows the top view of the detector, and the lower shows the side view. Red track indicates the true proton track, magenta means hit scintillator bars, blue has a hit with high photoelectron deposits, > 30. The proton energy for this event is 281 MeV/c. The pions are absorbed in iron, so the only proton makes visible hits in the scintillators. Photoelectrons deposited in the last four layers were 38, 31, 33 and 37, and $N_{p.e.}^{tail} \times \cos\theta_{\mu}$ was 113.5.

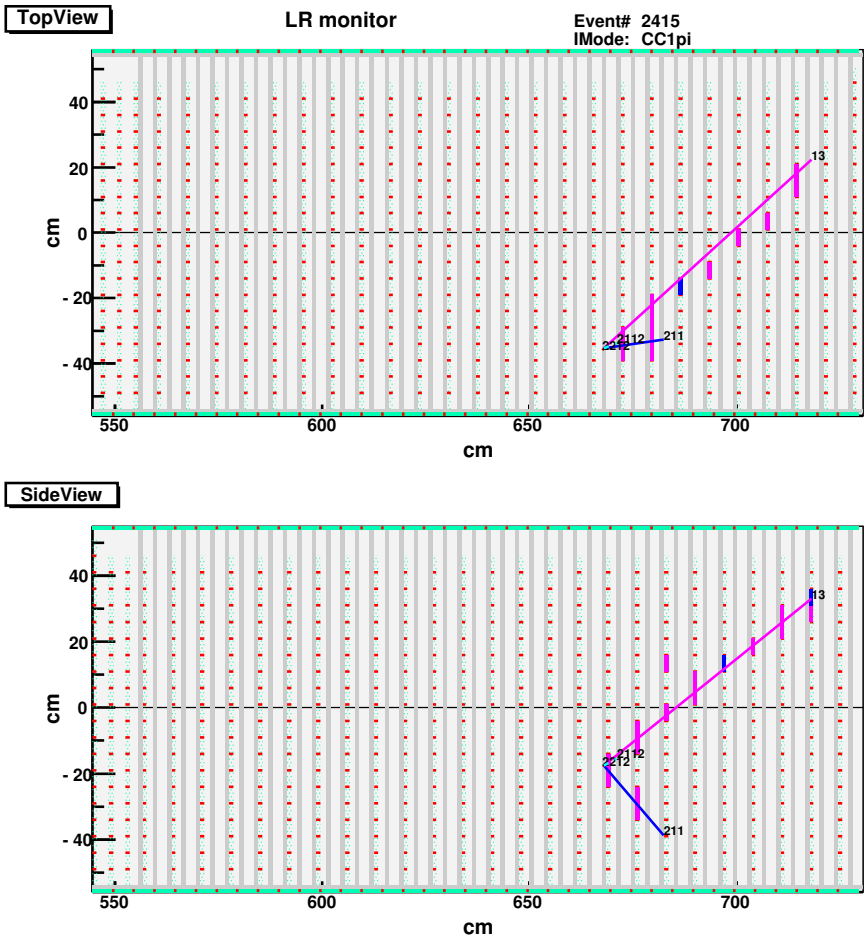

Figure 13: An event display of a multi-track event generated via a charged-current single pion interaction. Two tracks originated from a muon (labeled as "13") and a charged pion ("211") can be seen. There are multiple hit layers due to these charged particles.

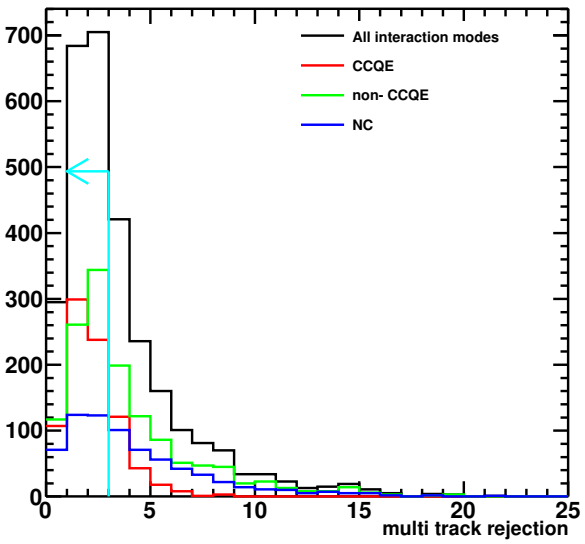

Figure 14: The number of layers having 2 or more hits ($N_{2HitLayer}$) distributions for each interaction mode. The $N_{2HitLayer}$ for CC non-QE events becomes larger than that for CC QE since non-QE events produce multi-tracks. In order to select single track events, $N_{2HitLayer} < 2$ is applied.

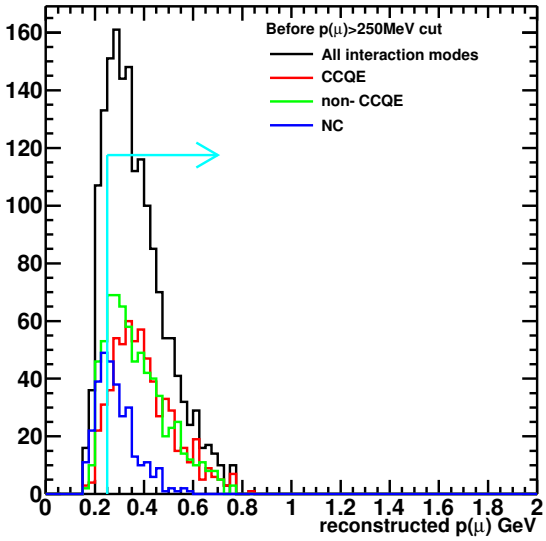

Figure 15: Reconstructed muon momentum p_μ[GeV/c] distribution for each interaction mode. The p_μ for NC events is reconstructed with mis-identification of proton as muon. Therefore, it tends to be lower. We applied $p_\mu > 250$ MeV/c to reject NC events.

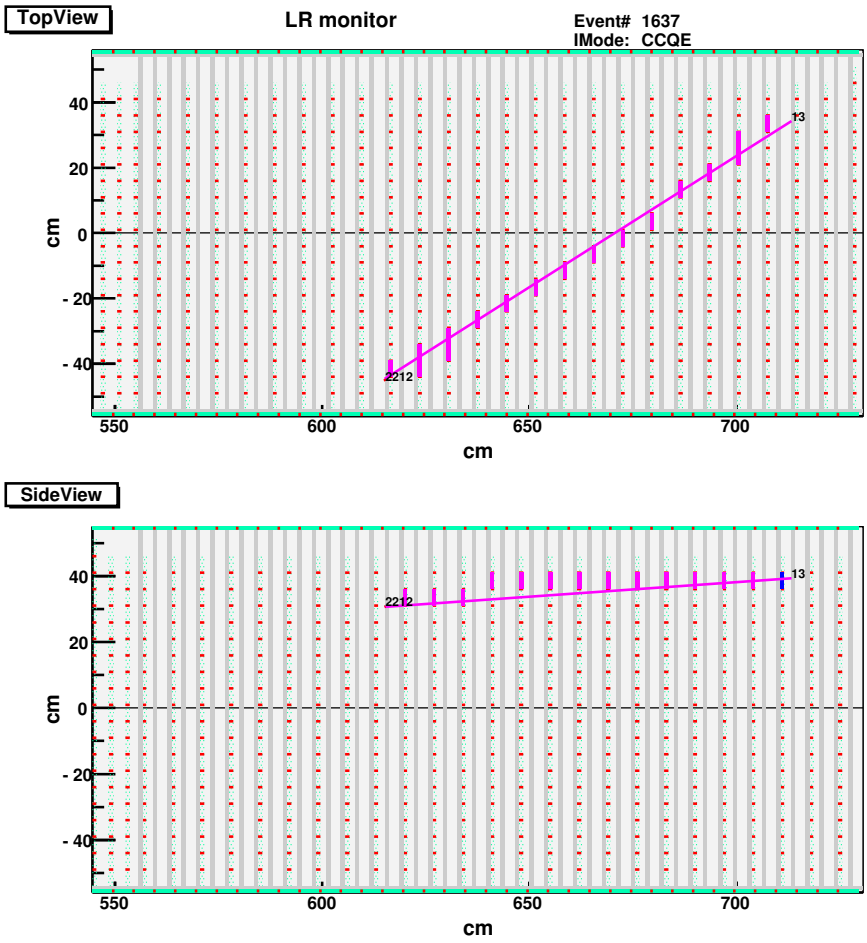

Figure 16: An event display of a typical CCQE event. A muon having 655 MeV/c momentum makes a clear single track and it reconstructed as a 644 MeV/c track.

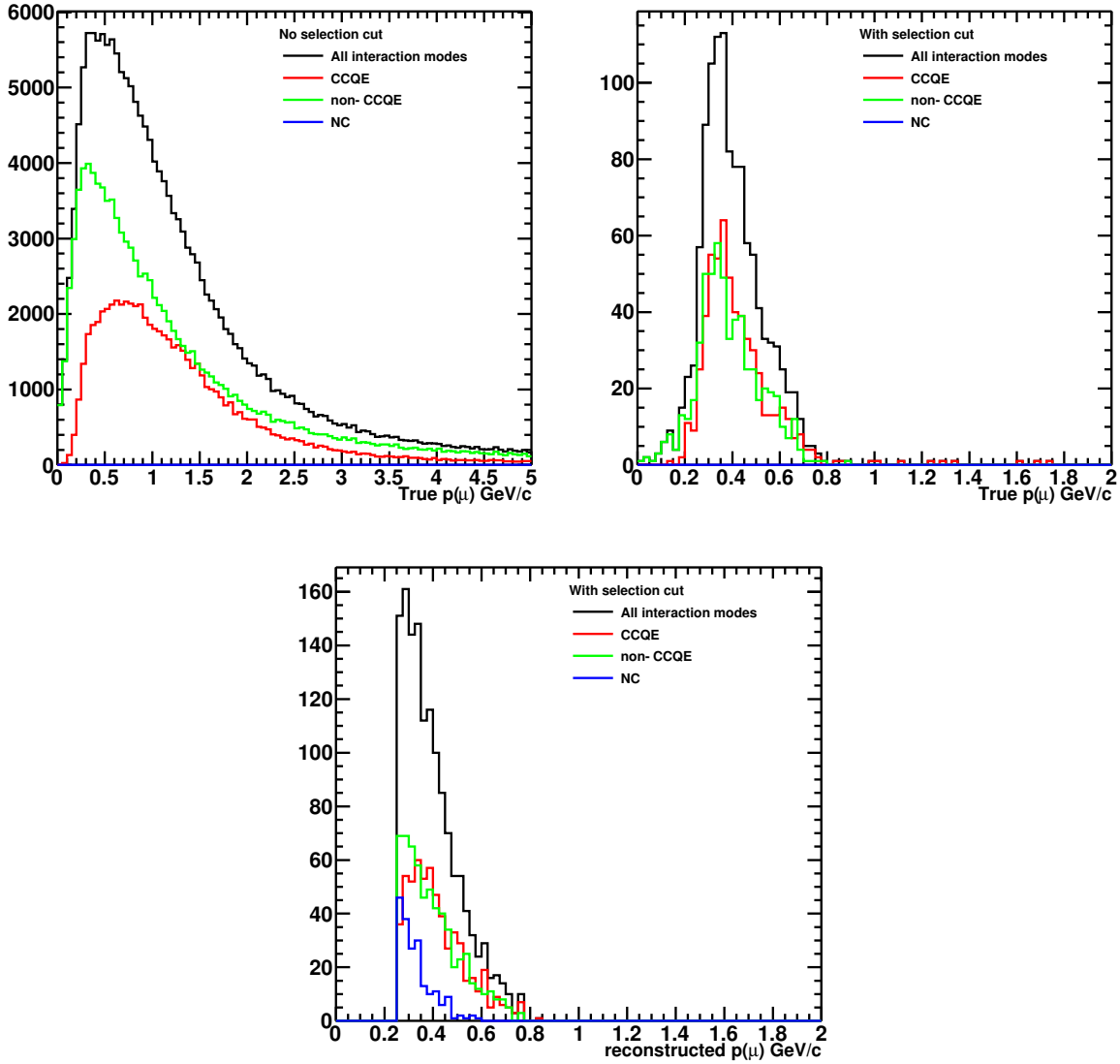

Figure 17: Distributions of the true muon momentum with no cut applied (top, left), after all the selection cuts (top, left). and the reconstructed one after all the cuts (bottom) are shown.

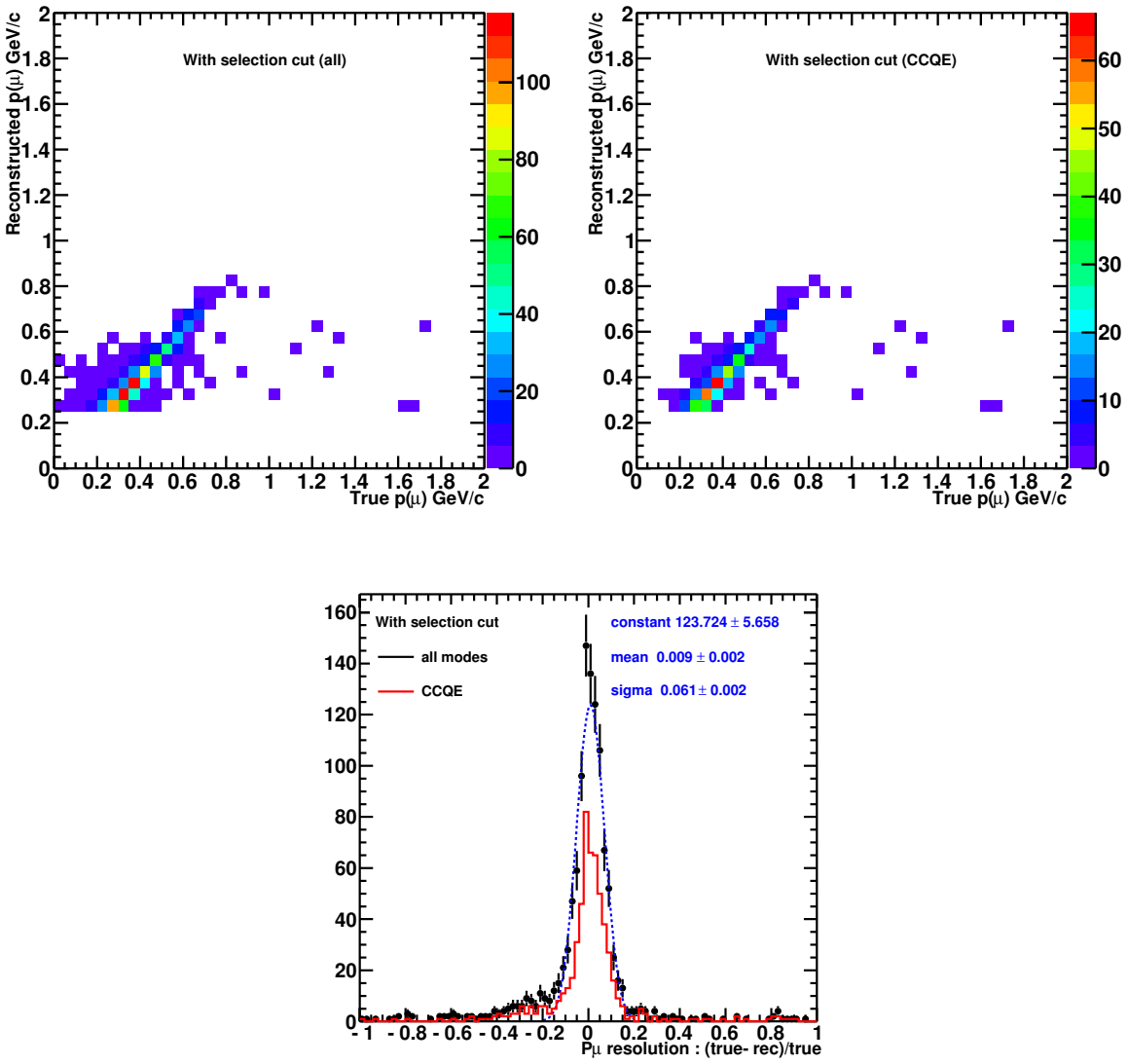

Figure 18: The reconstructed muon momentum as a function of the true muon momentum for the all surviving events (top, left) and the CCQE interaction mode only(top, right). The muon momentum resolution ($(true - reconstructed)/true$) is shown in the bottom. The resolution using all the interaction modes is 6% by fitting with Gaussian from -0.2 to 0.2.

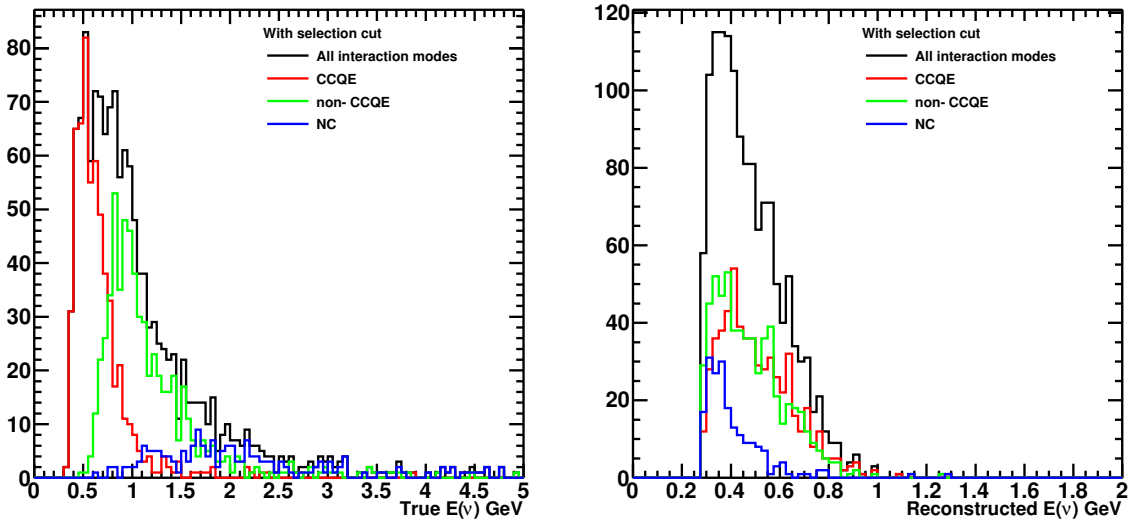

Figure 19: Distributions of the true (left) and the reconstructed (right) neutrino energy for each interaction mode.

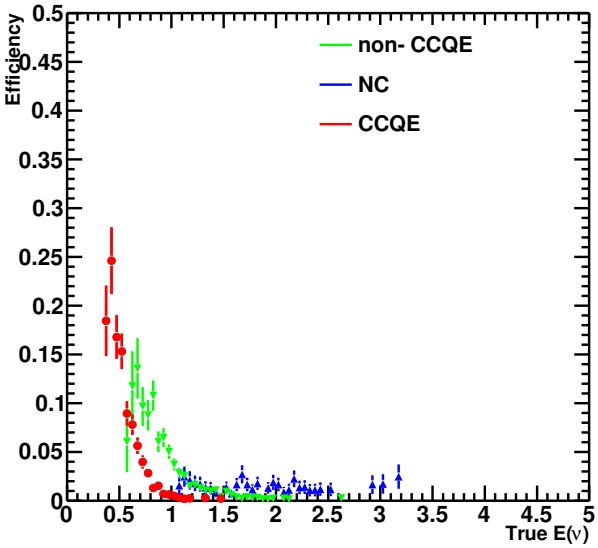

Figure 20: The event selection efficiencies as a function of the true neutrino energy for CCQE (red), CC non-QE (green), and NC (blue) interaction modes. The efficiency for the CCQE interaction events is higher than others below 1 GeV.

energy events. Only 1/60 of the events remain after no veto hit and track in FV requirements. In other words, the size of our detector is suitable for rejecting high energy events effectively. After applying all selections, the number of expected events assuming 100kW of proton beam intensity and 10^7 seconds of the running time is 3412. This means a 1.7 % accuracy in the measurement (statistical only). The purity of the CCQE events in the final sample is 42%. In spite of the low selection efficiency, sufficient statistics can be obtained in a year.

Table 1: The number of the surviving events after each step of selections. We assume 100 kW beam and 10^7 seconds of the running time. The numerator of the efficiency is the number of events having $N_{HitLayer} \geq 5$. The event fraction of each mode is summarized as well.

	All	CC	CCQE	non-CCQE	NC
No cut	629900	471610	166446	305164	158290
$N_{HitLayer} \geq 5$	418758	365722	125709	240013	53036
No veto hit	57107	36505	11237	25268	20602
In FV	17614	10521	3191	7330	7093
Proton track	7144	5416	2054	3363	1728
Multi track	4127	3348	1578	1770	779
$P_\mu > 250$MeV	3412	2929	1431	1497	483
Efficiency	0.0081	0.0080	0.0114	0.0062	0.0091
Fraction	1.	0.8584	0.4194	0.4387	0.1416

4 Construction and installation schedule

Most of the design and the assembling procedures have already been well established, and the detail will be finalized by the end of 2009.

We have already purchased all the scintillator bars, clear fibers, wavelength shifting fibers, and 64 channels multianode PMTs. The budget request for the electronics made by the Lyon group has also been approved. We intend to start purchasing the remaining materials (cookies, support structure, aluminum boxes, etc.) in early 2010. We will ship the scintillator bars and fibers from ICRR to Bern, then assemble the counter planes in Bern starting in March.

We will align 20 scintillator bars with fibers in an aluminum box and bundle the fibers with the cookie. This will take about one month. We will also perform simple tests using cosmic rays or sources. At the same time, ICRR will prepare the iron plates and the support structure, and Lyon will purchase all the electronics boards and boxes and prepare necessary DAQ software. These boards will be checked in Lyon before shipping them to ICRR.

We will ship the counter planes back to ICRR in May. We will assemble the counter and iron planes together at ICRR and perform the final cosmic ray test using the full DAQ system. This will be finished by July. We can store the detector at ICRR for a short period, if necessary.

If there is no conflict with other T2K near detector activities, we will be able to install the detector in the ND280m pit sometime in summer. Since the total mass should be less than 10 tons, and the installing area discussed in Section 1 has a direct access by the crane, installing and aligning can be done in one or two days, and we can start taking data shortly after.

We discussed with random people about the schedule and the location. There is no problem we heard so far.

We summarize the schedule as below:

Jan - Feb, 2010 Start to buy necessary materials.

March Start the production of the DAQ boards in Lyon. Send scintillator bars and fibers from ICRR to Bern.

April Assemble the counter planes in Bern. Prepare the frame structure and iron plates at ICRR.

May Send the counter planes back to ICRR. Commissioning of the electronics in Lyon.

June Receive planes at ICRR and assemble the full detector at ICRR. Cosmic ray tests.

July - August Ready to install.

5 Beam time request

We request 10^7 seconds of beam time under the assumption of 100kW beam power. Obviously, if the beam power would be higher, the exposure time will be reduced accordingly.

6 Conclusions

We propose a test experiment to measure low energy neutrino events with a simple detector system. By studying the possibility of performing an on-axis measurement of sub-GeV neutrino flux with our detector, we reached these conclusions:

- The detector discussed in this proposal can measure sub-GeV component of the beam with good performance and understand the beam characteristics with an integrated luminosity of 100kW for 10^7 seconds.
- After discussions with the relevant experts involved in the technical aspects of the ND280m installation and considering crane accessibility, smooth installation (and uninstallation) and the load tolerance of the floor, a suitable location for the detector 2.5m off-axis is identified that will not interfere with other activities in the ND280 pit.

We believe that the proposed detector can measure sub-GeV neutrinos at the J-PARC neutrino beam. The detector can be installed next summer with no conflicts with other detectors.

As a technical point of view, we have done physics simulation studies, built a prototype of the counter plane, tested with cosmic rays and confirmed that the full chain of the DAQ system works as expected.